Available online at www.sciencedirect.com
SCIENCE DIRECT®
International Journal of Thermal Sciences 45 (2006) 168–179
International Journal of Thermal Sciences
www.elsevier.com/locate/ijts

Gasoline direct injection spray simulation ☆

Rossella Rotondi *, Gino Bella

Università di Roma "Tor Vergata", Dipartimento di Ingegneria Meccanica, Viale del Politecnico 1, 00133 Rome, Italy

Received 23 November 2004; received in revised form 1 June 2005; accepted 1 June 2005

Available online 28 July 2005

Abstract

In this paper the problems related to mixture formation in a GDI engine are analyzed. The atomization of a hollow cone fuel spray generated by a high pressure swirl injector is studied by means of a numerical technique. The model distinguishes between primary atomization and secondary breakup. The latter was modeled, as done in a previous work on Diesel atomization, using different mechanisms as the droplet Weber number changes. At first the spray atomization in a quiescent chamber, at ambient pressure and temperature, was considered. The validation of the model was made comparing the numerical penetration and spray morphology with experimental results. Combustion simulations were also performed comparing numerical results with experimental data of a GDI (Gasoline Direct Injection), 4 stroke, 4 cylinder, 4 valves per cylinder engine. Such simulations were made to analyze and understand the mixture formation mechanism in both stoichiometric and stratified operation mode. The results show how, the interaction between the air motion and the fuel spray, leading factor in spray atomization, is fundamental to realize an efficient mixture formation and combustion locally very lean, typical of stratified charge combustion.

Keywords: Gasoline direct injection; Atomization; Swirl atomizer; Droplet breakup; Combustion

1. Introduction

In the last twenty years the fuel system of spark ignition (SI) engines has evolved monotonically from carburetion to throttle-body injection, then to simultaneous-fire port-fuel injection (PFI), and more recently to phased sequential-fire PFI. Advanced systems such as variable valve-timing, multiple roller camshaft, computer algorithms for transient metering, turbocharging have also been incorporated. But the current high-technology PFI engine, although highly evolved, has nearly reached the limit of the potential since it still uses throttling for load control and it still has a film of liquid fuel in the intake ports. The gasoline direct injection (GDI), in theory, does not have these two limitations and offers many opportunities for achieving significant improvements in engine fuel consumption and emissions reductions [1,2].

To satisfy CO_2 emissions restrictions that will be introduced in the industrialized countries, Brake-specific fuel consumption (BSFC) has to be reduced. Gasoline port-fuel injection engine that are in production today have an higher BSFC compared to the direct-injection (DI) Diesel engine. This is due to the higher compression ratio and the unthrottled operation typical of diesel engines, that, however, have higher NO_x and soot emissions, slightly higher noise level and lower startability. The ideal would be to put together the best features of the both combining Diesel efficiency with gasoline specific power. Studies in this direction have shown that this may be achieved with gasoline direct injection (GDI) unthrottled engine. Fuel is injected directly into the combustion chamber in order to have a mixture with an ignitable composition near the spark plug at the time of ignition for all loads. Power is controlled by varying the amount of fuel injected in a diesel-like manner, and with the unthrottled operation pumping losses are significantly reduced. Because of the charge cooling during injection higher com-

☆ A preliminary version of this paper was presented at CHT-04: An ICHMT International Symposium on Advances in Computational Heat Transfer, April 2004, G. de Vahl Davis and E. Leonardi (Eds.), CD-ROM Proceedings, ISBN 1-5670-174-2, Begell House, New York, 2004.

* Corresponding author.
E-mail addresses: rossella.rotondi@uniroma2.it (R. Rotondi), bella@uniroma2.it (G. Bella).

1290-0729/$ – see front matter
doi:10.1016/j.ijthermalsci.2005.06.001

Nomenclature

C_D	drag coefficient
$\overline{D}$	characteristic size of Rosin–Rammler distribution function
d	diameter
F	ratio between the amplitude of the pressure waves that arise in viscous flow over those in a unviscous flow
h	sheet thickness
K	discharge coefficient
L_b	break-up length
Oh	Ohnesorge number
p	pressure
q	exponent of the Rosin–Rammler distribution
t	time
$\bar{u}$	velocity
U	magnitude of ligament velocity
We	Weber number
X	orifice-air core area ratio

Greek symbols

α	hollow cone angle
β	thickness angle
θ	spray angle respect to the injector axis
λ	mixture equivalence ratio
ρ	density
σ	surface tension

Subscript

0	initial
amb	ambient
D	droplet
g	gas
h	ligament
inj	injection
l	liquid
n	normal direction
noz	nozzle
r	relative (gas–liquid)

pression ratio, lower octane requirement and increased volumetric efficiency lead to an improved BSFC up to 30%.

There can be different degrees of design complexity for a GDI engine:

(1) The simplest one is an engine that operates in the early injection homogeneous stoichiometric mode, that uses throttling for load control. It doesn't use the potential associated with throttle elimination but still takes the advantages of charge cooling and more rapid startability.
(2) The next level would be an engine that uses a leaner homogeneous mixture with reduced throttling for some degree of load control.
(3) The last is the full GDI concept: unthrottled, using a overall lean stratified mixture at part load, obtained with a late injection, that smoothly passes to a homogeneous full load mixture by injecting increased volumes of fuel early in the cycle.

The most complex would operate in all three modes at various times, requiring complex control system ad reliable sensors. The realization of highly stratified GDI combustion chambers is one of the hardest task, where the critic step is the stratification at partial loads, at which, an erroneous mechanism of mixture formation leads to an increase of engine specific consumption and unburned hydrocarbons emissions [3,4].

2. From port fuel to direct injection gasoline engines

In the PFI engine, the gasoline is injected into the intake port of each cylinder mostly onto the back of the intake valve when it is closed. The injector is mounted either in the cylinder head upstream of the intake valve or in the intake manifold near the cylinder head. During cold start a transient film of liquid fuel is formed in the intake valve area of the port, and some portion of it is drawn into the cylinder during each induction event. So the fuel delivered to the cylinder in each cycle differs from that metered by the injector. This causes a fuel delivery delay and an associated inherent metering error due to partial evaporation. This makes necessary to supply extra fuel for cold start, that exceeds the stoichiometric value, so that an increase of engine-out emissions of unburned hydrocarbons is experienced [1].

In a GDI engine, the fuel is injected directly into the cylinder avoiding the problems related with fuel film in the port. However this does not guarantee that fuel film problems are absent: the wetting of the piston crown or other combustion chamber surfaces, whether intentional or not, may occur. The mass delivered into the cylinder is more accurately controlled, providing potential for leaner combustion and less cycle-to-cycle variations. GDI engines requires much less fuel to start leading to reductions in hydrocarbons spikes during transient operations, that could approach the level observed for steady operating conditions [5]. Other advantages of the GDI are the fuel cut-off in deceleration and the cooling of the inducted charge. The evaporation of the fuel droplets cools the air and this allows higher compression ratios and lowers the octane requirement of fuels, and, in addition, if the injection occurs during the induction event also the volumetric efficiency can be enhanced. Another limitation of PFI is the use of throttling for load control, that in the GDI engine is obtained varying the amount of fuel injected.

In spite of the potential advantages mentioned above the development of GDI engines has encountered many obstacles that hinder its application. The injection of fuel in the cylinder reduces the time available for evaporation and mixing. The PFI engines have the advantage that the intake system acts as a prevaporizing chamber. In GDI engines the time is reduced so fuel spray atomization has to be an order of magnitude finer, so that higher injection pressures are necessary. Moreover the high NO_x and HC (that represent a significant research problem to be solved) emission at high load, higher particulate emissions and the fact that a three way catalyst cannot be effectively used. Even if the engine operates at an overall lean condition that reduces NO_x emission the level is still high compared to the level obtained with a three way catalyst, so much work has been made and is still needed to develop lean NO_x catalyst. The most important obstacle in the development of GDI engines is that the control of the stratified-charge combustion over the entire operating range is very difficult. Since the location of the ignition source is fixed in SI engines the mixture cloud must be controlled both temporally and spatially for a wide range of operating conditions. The development of a successful combustion system depends on the design of the fuel injection system and the matching with the in-cylinder flow field.

Fuel injection system. The fuel injection system needs to provide different operating modes for the different loads. Fuel injection pressure vary in a range from 4 to 13 MPa (the actual trend is to increase the level of pressure), which are low if compared to diesel applications (50–160 MPa) but still high in comparison with PFI values that range from 0.25 to 0.45 MPa. These higher pressure values allow a higher penetration and reduce the mean droplet diameter determining a better atomized spray and a good penetration. Too high injection pressures will enhance atomization but at the same time produce a overpenetrating spray and wall wetting problems, especially when a sac volume is present. For the unthrottled part-load case, a late injection is needed in order to allow stratified charge combustion, with a well atomized compact spray to control the stratification. The fuel is injected during the compression stroke when the cylinder pressure is about 0.2–1 Mpa, which requires a relatively higher injection pressure compared to the full-load case. In the full-load case a stratified homogeneous charge is needed and this is done with a early injection, during the induction. A well dispersed spray is desirable, with bigger cone angle and a conical shape. To improve the transition between the two modes a split injection during the intake and compression stroke may be used.

As mentioned before the higher injection pressure are necessary to reduce the Sauter mean radius (SMD) of the liquid spray, because the fuel must vaporize before the spark event occurs in order to limit UBHC emissions and to have a repeatable ignition process. The smaller the droplet size the faster the vaporization occurs. GDI systems require fuel droplets of under 20 μm SMD, whereas PFI can operate well using sprays of 120–200 μm SMD. On the other hand Diesel engine require SMD lower than 8 μm. The SMD itself is not sufficient to classify spray atomization respect to UBHC emissions, spray drop size distribution must not have a wide spread because even a small percentage of bigger droplets, not evaporating completely, may effect the UBHC emissions. To better characterize the spray size distribution the DV90 statistic may also be introduced, which is a quantitative measure of the largest droplets in the spray. It is the droplet diameter corresponding to the 90% volume point, so it gives a measure of the droplet size distribution spread.

GDI injectors can either be single fluid or air-assisted (two phase) and may be classified by atomization mechanism (sheet, turbulence, pressure, cavitation), by actuation type, nozzle configuration (that can be either swirl, slit, multihole or cavity type), or by spray configuration (hollow-cone, solid-cone, fan, multi-plume). A detailed classification of GDI injectors may be found in [1] and in Table 1 the classification categories are reported [1].

Currently the most widely used injector for GDI applications, that is the one analyzed in this paper, is the single-fluid, swirl-type unit, that uses an inwardly opening pintle, a single exit orifice and a fuel pressure, in the range of 7–10 MPa, schematized in Fig. 1 [6].

Table 1
Classification categories for GDI injectors [1]

Primary atomization method	Actuation mechanism	Spray configuration
Sheet (swirl-type)	Single solenoid	Hollow-cone
Pressure (hole-type)	Dual-solenoid	Solid-cone
Pressure(slit-type)	Piezoelectric	Fan
Turbulence (compound plate)	Hydraulic	Offset
	Cam	Shaped
		Multi-plume
Nozzle configuration	Pintle opening direction	Fluid state
Swirl	Inwardly opening	Air-assist (two-phase)
Slit	Outwardly opening	Single fluid
Multihole		
cavity		

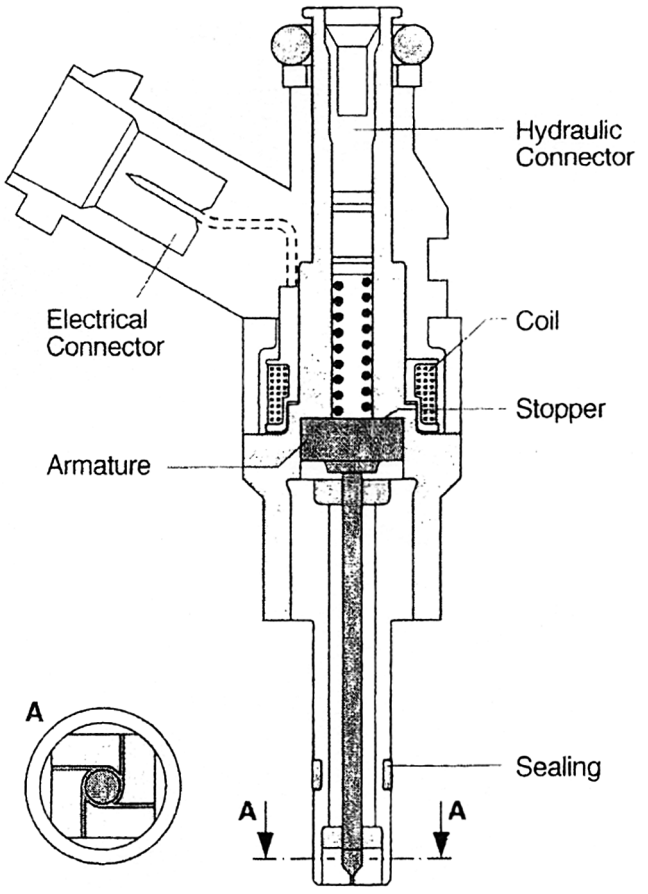

Fig. 1. Schematic of inwardly opening, single-fluid, swirl-type injector [9].

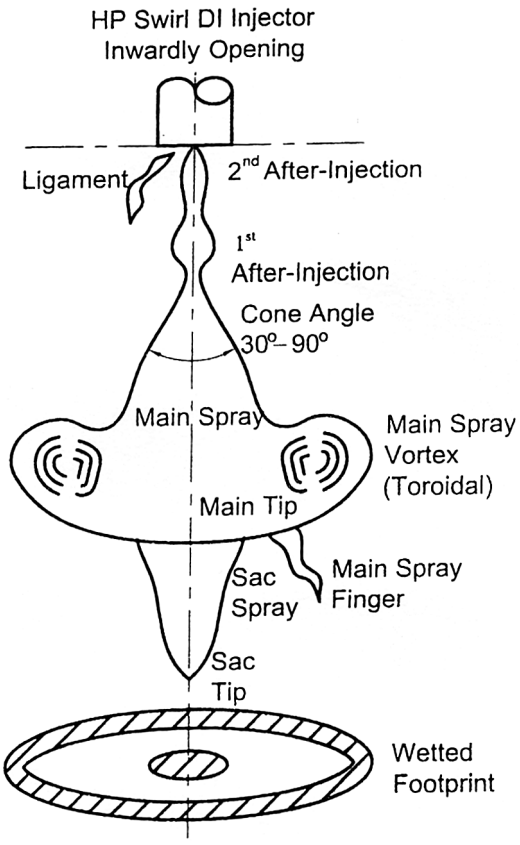

Fig. 2. Schematic representation of a HP Swirl GDI Injector Inwardly opening.

The liquid emerges from the single discharge orifice as an annular sheet that spreads radially outward to form an initially hollow-cone spray. Pressure energy is transformed into rotational momentum that enhances atomization. The initial spray angle ranges between 25°–150° and SMD varies from 14–23 μm. It produces a spray with a narrower distribution of drop sizes (DV90–DV10) than the one obtained from a standard hole-type nozzle. Surface roughness may, however, produce streams of fuel in the fuel sheet, resulting in formation of pockets of locally rich mixture. A schematic representation of features in a typical in this type of injector are reported in Fig. 2 [1].

The spray has a leading edge (the main spray tip) that penetrates away from the nozzle tip for about 50 mm in less then 20 ms. A Toroidal vortex is also attached to the periphery. The leading edge of the spray contains a separate sac spray.

3. Numerical computation tool

The developed numerical computation tool “NCF 3D” is based on the well known KIVA III code originally developed by the Los Alamos Laboratory [7,8]. The original version employs a finite volume approximation of the governing 3D Navier–Stokes (N–S) equations in a Cartesian or cylindrical reference system in which a multi-block grid structure is generated. A modified k–ε turbulence model, accounting for compressibility effects, is used during the arbitrary Lagrangian Eulerian (ALE) integration of the averaged N–S equations. The original version has been enhanced by a certain number of specific submodels necessary for the computation of the dynamic fuel spray behavior, including spray atomization, gas phase motion as well as combustion. The GDI specific enhancements of the NCF 3D code can be listed as follows:

(1) Introduction of the experimentally obtained initial spray formation characteristics (spray angle and main axis direction, initial droplet diameter and position in the spray, initial droplet velocity) [9].
(2) Improvements of the formulation of the gas/wall heat transfer model in order to deal with transient effects and compressibility. The re-writing of the submodel follows the approach suggested in [10,11].
(3) Implementation of a droplet wall interaction submodel [12].
(4) Implementation of a spark initialization submodel [13].
(5) Introduction of a law for the turbulent characteristic time scale [13,14].
(6) Implementation of a characteristic time combustion model [15]

All this items have been discussed in detail in previous papers [9,13] thus the enhanced spray formation and atomization model will be presented in the following.

4. GDI spray atomization models

Spray formation and initial conditions. A Lagrangian treatment of stochastic particle injection is used for the liquid drops that simulate the spray. The fuel spray enters the computational domain as an annular sheet, but in the KIVA spray model this continuous liquid is artificially divided into discrete Lagrangian parcels injected into the gas. Each computational parcel represents a group of physically similar droplets that exchange mass momentum and energy with that surrounding air through source terms in the gas phase equations. The liquid jet is simulated injecting blobs with characteristic size equal to the sheet thickness as shown in Fig. 3.

The sheet injection velocity is evaluated by means of:

$$\bar{u}_{\text{inj}} = K\left[\frac{2(p_{\text{inj}} - p_{\text{amb}})}{\rho_l}\right]^{0.5} \tag{1a}$$

$$K = \frac{C}{\cos\beta}\sqrt{\frac{1-X}{1+X}} \tag{1b}$$

$$X = \left(1 - \frac{2\cdot h}{d_{\text{noz}}}\right)^2 \tag{1c}$$

C is a constant, X is the orifice-air core area ratio, d_{noz} the diameter of the nozzle and h is the sheet thickness given by Risk and Levebvre [16]. In order to take into account the initial phase of the spray (pre-spray), the angle α is supposed to vary, during the injection phase, as reported in Fig. 4. The injection timing, $\Delta t_1 = 50$ μs, $\Delta t_2 = 400$ μs and the maximum value of angle $\alpha_{\max} = 75°$ have been evaluated starting from experimental data.

For GDI spray atomization two different approaches may be found in literature:

Han and Reitz primary atomization model [17]. In a previous work [18] the atomization model by Han and Reitz has been used. In this approach the break-up of the liquid sheet is studied on the basis of the stability analysis of sinuous wave

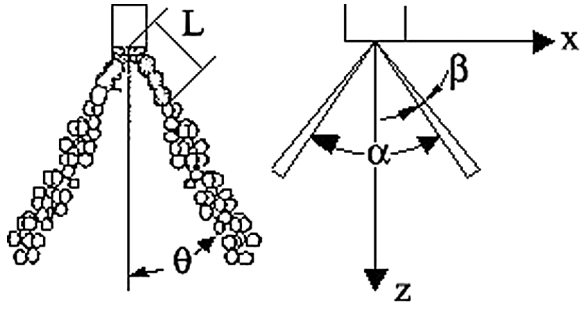

Fig. 3. Schematic of the hollow cone discretization and definition of spray parameters.

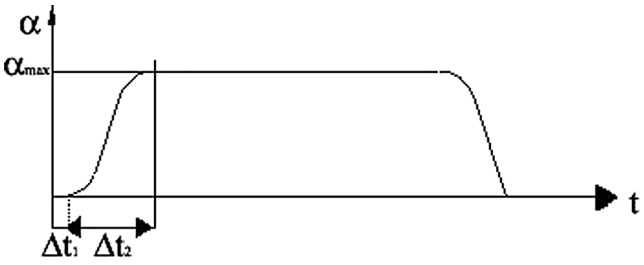

Fig. 4. Variation of the angle α during the injection phase.

on the conical sheet. A suitable equation, which calculates the break-up length L_b, can be deduced from [17]:

$$L_b = B\left(\frac{\rho_l \sigma_l h \cos\theta}{\rho_g^2 u_r^2}\right)^{1/2} \tag{2}$$

where B is a constant, ρ_{g} the environmental gas density, σ_{l} the liquid surface tension coefficient and u_r the magnitude of the sheet-gas relative velocity. The liquid blobs, after the length L_{b}, break-up according to the KIVA 3 break-up model, modified as suggested by [17]. The product drops after the blob break-up and the blobs located at a distance from the nozzle greater than the sheet break-up length L_{b}, are treated as secondary droplets affected by drag forces and gas turbulence.

Nagaoka and Kawamura primary atomization model [19]. The liquid jet exiting the injector is treated as a liquid *sheet* till it reaches its breakup length. The *sheet* is analyzed discretizing its volume in small quantities and applying to them the momentum conservation equation:

$$\frac{\mathrm{d}\bar{u}_l}{\mathrm{d}t} = C_D \frac{\rho_g |(\bar{u}_g - \bar{u}_l)_n|}{\rho_l}(\bar{u}_g - \bar{u}_l)_n + \frac{1}{\rho_l}\frac{\partial p}{\partial n} \tag{3}$$

in which C_D is the drag coefficient, $\bar{u}_g$ is the velocity vector related to the gas comprehensive of the turbulence term (for which the k–ε model implemented in KIVA was used), $\bar{u}_l$ is the velocity vector related to the liquid "*sheet*". Subscript n refers to the sheet normal direction. The variation of the *sheet* thickness during the injection period, is evaluated imposing mass conservation:

$$h = \frac{K_0}{L + K_0/h_0}, \quad K_0 = h_0(d_0 - h_0)\cos\theta/(2\sin\theta) \tag{4}$$

where θ is the angle respect to the injector axis and h_0 represents the sheet thickness at the exit of the injector [20]. The breakup length is evaluated by means of the formula [21]

$$L_b = \frac{18\sqrt{2}}{F}\sqrt{\frac{\rho_l}{\rho_g}}\frac{h}{\sqrt{We_h}} \tag{5}$$

where We_h is the Weber number of the ligament and F is the ratio between the amplitude of the pressure waves that arise in viscous flow over those in a unviscous flow evaluated as follows:

$$F = \sqrt{N(2-N)}\left[\left(1 + \frac{N^3V^2}{4(2-N)}\right)^{3/2} - \frac{3}{2}\sqrt{\frac{N^3V^2}{4(2-N)}}\right]$$

$$F \approx (1 + 2.29V)^{-0.677}$$
$$V = \frac{\sqrt{2}}{4} Oh\, We_h = \frac{\mu_L \rho_g U^2}{2} \sqrt{\frac{h}{2\rho_L \sigma^3}}$$
$$Z = Oh\, We_h$$
$$Oh = \mu_h / \sqrt{\rho_L \sigma h}$$
$$We_h = \rho_g U^2 h / \sigma \tag{6}$$

where U is the magnitude of the *ligament* velocity.

Before the droplet detaches from the liquid sheet, because of the interaction between the two phases, *ligaments* form on the surface. *Ligaments*, of characteristic size d_h, are formed on the conical sheet, due to the interaction with the surrounding air:

$$d_h = \left(\frac{8}{9}\right)^{1/3} \left[\frac{K_0^2 \sigma^2}{\rho_g \rho_l U^4}\right]^{1/6} \times \left[1 + 2.6\mu_l \left(\frac{K_0 \rho_g^4 U^7}{72\rho_l^2 \sigma^5}\right)^{1/3}\right]^{1/5} \tag{7}$$

These *ligaments* detach as droplets whose diameter is given by a Rosin–Rammler distribution function [22]

$$1 - V = e^{-(d_D^q / \overline{D})} \tag{8}$$

with characteristic size $\overline{D}$ related to the *ligament* size by the following correlation:

$$\overline{D} = C_1 1.88 d_h (1 + 3Oh_h)^{1/6} \tag{9}$$

in which Oh_h is the Ohnesorge number of the *ligament* ($Oh_h = \mu_l / \sqrt{\rho_l \sigma d_h}$) [23].

Eq. (8) is widely used in spray applications, to determine the post breakup sizes of the primary parcels. Usually for internal combustion engines applications $1.5 < q < 4$, and was put equal to 3.5 as stated in [17]. As stated in [24] C_1 is an empirical factor, put equal to 1. In present simulation this model was used for primary atomization as done in previous work [25].

Secondary breakup model. A new droplet secondary breakup model was developed in previous work for Diesel applications [26]. The droplets formed after the atomization of the annular liquid sheet, may undergo secondary breakup. Because of the forces acting on a droplet, as it moves in the surrounding gas, a non-uniform pressure distribution is developed around it. This process leads to droplet deformation and subsequent breakup. The relevant forces in this physical phenomenon are those related with surface tension, viscosity, inertia and surface instabilities responsible for wave growth. Rayleigh–Taylor instabilities may occur at drop windward surface when a body force is directed normally to the interface of the two fluids from the more dense to the less dense one. Kelvin-Helmholtz instabilities are due to the shear forces in the relative parallel motion at the common interface. Different regimes can be observed as the relative magnitude of these forces varies. One possible classification [27] can be made over different ranges of droplet Weber number ($We = \rho_l u_r^2 d_D / \sigma_l$):

- $We = 12$ *Vibrational mode:* Fragmentation is caused by the amplification of droplet deformation originated by vibrational resonance of liquid surface;
- $12 < We < 45$ *Bag regime:* Drop breakup is due to the deformation of the droplet in a bag-like structure that disintegrates after a critical value of deformation is reached (Fig. 5(a));
- $45 < We < 100$ *Chaotic regime:* A transitional regime in which droplet breakup is due to both ballooning and breaking of filaments resulting from the liquid surface layer ripping;
- $100 < We < 1000$ *Stripping regime:* The flow over the drop causes the ripping of the surface inducing a thin laminar boundary on it. After a certain stage of deformation, the boundary layer is stripped from the periphery because of K–H instabilities effects, in the form of film and fragments (boundary layer stripping). Drop diameter gradually reduces and, when a critical value is reached, the drop disintegrates in smaller ones with bimodal distribution (Fig 5(b));
- $We > 1000$ *Catastrophic regime:* At very high Weber number both R–T and K–H instabilities are involved. The first, due to droplet deceleration and related with higher values of wavelength and amplitude, lead to the formation of bigger drops then those related with K–H instabilities associated with lower values of wavelength and amplitude (Fig. 5(c)).

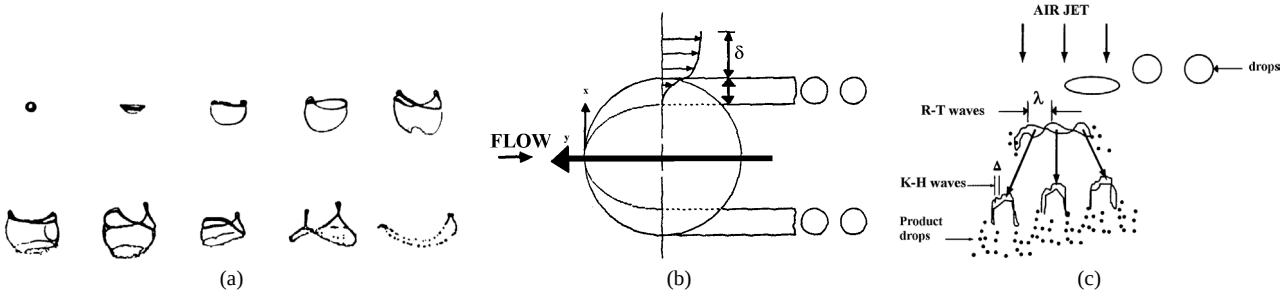

Fig. 5. (a) Droplet deformation and breakup in the bag regime [27]; (b) Boundary layer stripping [28]; (c) Competition between R–T and K–H instabilities in the catastrophic regime [28,29].

For GDI pressure system the injection velocities can reach maximum values of about 100 $m \cdot s^{-1}$, so the Catastrophic regime is unlikely to happen. During their lifetime drops may decelerate, breakup, evaporate and a different ranges of droplet Weber number can be reached, so different secondary breakup mechanism can then be simultaneously present.

The WAVE [30] model is based on a stability analysis of liquid jets and can be used to simulate the primary atomization of liquid core in the regimes in which jet breakup is governed by aerodynamic interaction with air (low-medium injection pressure case).

The TAB [31] and DDB [32] model are based on the dynamic of single droplet and can be therefore considered as secondary breakup model. In the first the breakup is due to the amplification of droplet deformation resulting from vibrational resonance of the surface and therefore was chosen to model droplet breakup in the Vibrational regime. The latter is a deformation-induced secondary breakup model and used in the Bag regime. The WAVE model considers K–H instability effects and can be used to simulate the breakup of secondary droplets in the Stripping regime and in the Catastrophic one in competition with the RT model. The R–T model considers Rayleigh–Taylor instabilities that arise on very high speed droplet surface and therefore can be adopted to model droplet secondary breakup in the catastrophic regime in competition with a K–H instability based model (WAVE). In the Chaotic regime, in which bag breakup and stripping coexist, a competition between the DDB model and the Wave model was implemented.

All the models are used with the original value of the constants except for the WAVE model. For the latter customized value of the size constant ($B_0 = 0.59$) was chosen, while the time constant B_1 was set equal to 80 according to previous work [33,34] in which the values of the constants were determined for the low injection pressure range, comparing numerical droplet sizes and velocities to the experimental ones evaluated by means of a phase Doppler particle analyzer (PDPA) technique.

The injected blobs are treated as primary blobs and are processed by the primary breakup model. After breakup it is treated as secondary droplet and is processed by one of the secondary breakup model according to its Weber number, as listed in Table 2.

Table 2
Atomization model

Atomization model	
Primary breakup	
GDI Hollow cone injector	Nagaoka et al.
Secondary breakup	
$12 < We < 16$ (vibrational)	TAB
$16 < We < 45$ (bag)	DDB
$45 < We < 100$ (chaotic)	DDB + WAVE
$100 < We < 1000$ (stripping)	WAVE
$We > 1000$ (catastrophic)	WAVE + RT

5. Spray results

The atomization model was tested comparing numerical and experimental data. Tests were made injecting gasoline in a quiescent chamber (0.1 MPa pressure, 300 K temperature). Such conditions, if not considering the absence of a well developed flow field, are not that far from the in-cylinder ones since the injection starts during the intake stroke at the beginning of compression.

The spray is of a hollow cone type and the injector is fuelled by a displacement pump that compresses the fuel up to 10 MPa. For the tests a computational grid of 3 mm spacing was used. The results are presented in terms of comparison between the numerical and experimental tip penetration and a comparison of the spray morphology at different time steps. The tip penetration is determined by the pre-spray that is injected with a very small cone angle compared to the maximum value (90°) and with a value of velocity near to the maximum. The variation of spray cone angle and injection velocity are evaluated experimentally and given to the code as spray model initial conditions. Comparing numerical and experimental tip penetration it is evident how the code well predicts this macroscopic quantity (Fig. 6). Initially they both have a linear trend which becomes parabolic due to the drag effects, subsequently the atomization of the sheet produces many small droplets increasing the exchange surfaces between air and liquid. All this phenomena are well modeled determining a discrepancy between the numerical and experimental values of less then 2%.

Concerning the secondary breakup, due to the low Weber numbers of the detached droplets, only the vibrational and bag regime occur, as shown in Fig. 7, in which the occurrence factor of each regime is reported against time. The occurrence factor of each regime at a specific timestep is defined as the number of secondary droplets "breaking up" in that regime over the total number of "broken" drops in that timestep.

In Fig. 8, the numerical and experimental spray images are reported. The darker numerical parcels are plotted over

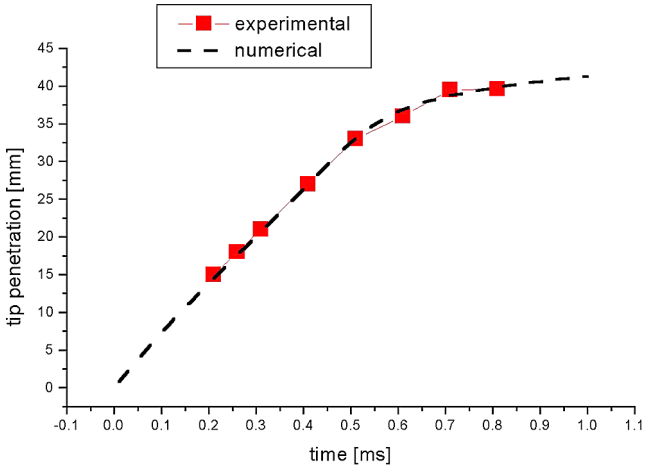

Fig. 6. Numerical and experimental tip penetration versus time.

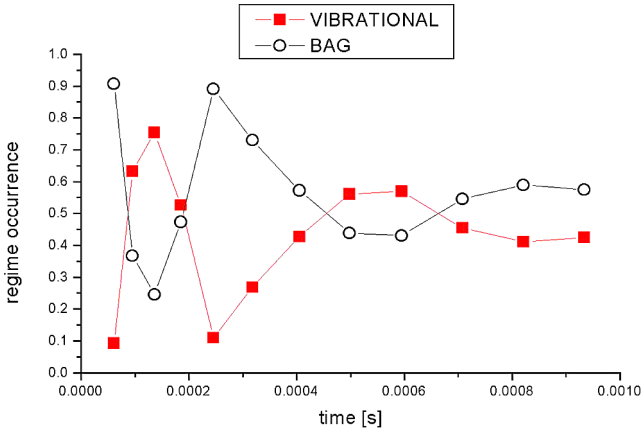

Fig. 7. Occurrence factor of different secondary breakup regimes.

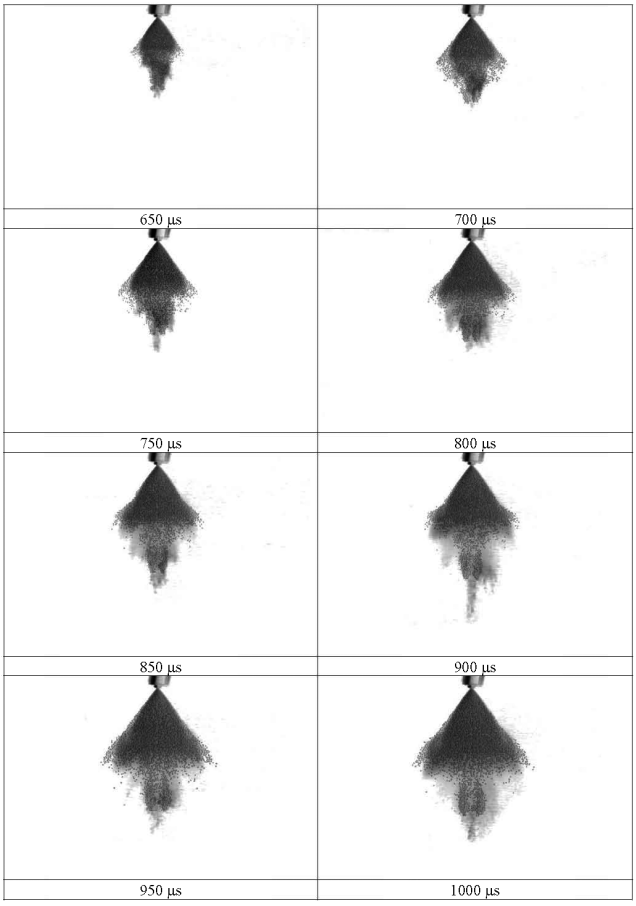

Fig. 8. Experimental and Numerical Spray morphology.

the lighter experimental spray. The experimental pictures are obtained by means of a CCD camera synchronized with a laser light pulse at different time steps. All the images show a good correlation between the numerical and experimental spray. The breakup length at which the primary blobs start to breakup can be noticed. The evolution of the pre-spray is very important in determining the penetration. From the figures, at the latest time steps, small secondary droplets at the periphery of the jet can be noticed. These are characterized by small diameter and Weber number and are like floating in the surrounding air and are carried up by the flow field.

Table 3
Basic engine geometric characteristics

Bore	7.2 [cm]
Stroke	10.2 [cm]
Displacement	459.5 [cm^3]
Number of cylinder	4
Compression ratio	12.5

6. Engine results

The numerical code has been tested comparing numerical results with experiments on a GDI, 4 cylinder, 4 valves per cylinder, whose characteristics are reported in Table 3 [35].

This engine is fuelled by the injector previously described. Compared to a MPI engine it is characterized by an higher compression ratio typical of this class of engines. As load changes the combustion varies from stratified to homogeneous as previously described. To predict correctly the combustion phase a precise mixture formation modeling is therefore necessary, so present simulation must involve also the intake and exhaust stroke to have a right prediction of the air motion inside the cylinder which highly influences the mixture formation. For this type of engines the homogeneous charge is not to be intended as perfect mixing between fuel and air but as stoichiometric ratio of the two. The engine, as it can be evinced from the CAD design of Fig. 9, has in the intake ducts of each cylinder a valve able to modify the air motion in the cylinder as a function of the engine operating conditions. For the full load case, requiring an homogeneous charge, the above mentioned valve is completely open determining a well organized tumble motion in the cylinder, while at part load, when a stratified charge is needed, the valve is throttled in order to have a swirl motion in the chamber.

As the grid generation sometimes can be a rather long and tedious operation a specific approach involving several industrial codes has been made. For this kind of fluid-mechanic computation, a very detailed grid is absolutely necessary. This is why the grid generation is performed directly within the main frame of the original design in CAD-CATIA , while the final multi-block mesh for the KIVA III solver is made by the IBM created interface, the ENGAGE code [36]. The resulting computational domain is shown in Fig. 10. The grid has about 160.000 computational cells and discretizes the cylinder and part of the intake and exhaust systems. An extra volume is added at the beginning of the intake system to provide a boundary condition similar to the real engine plenum. The fluid-dynamic solver is of a multi-block type, requiring long work for domain decomposition. A lot of work has been done to asset the subroutine for the moving grid boundaries.. All the obtained results are

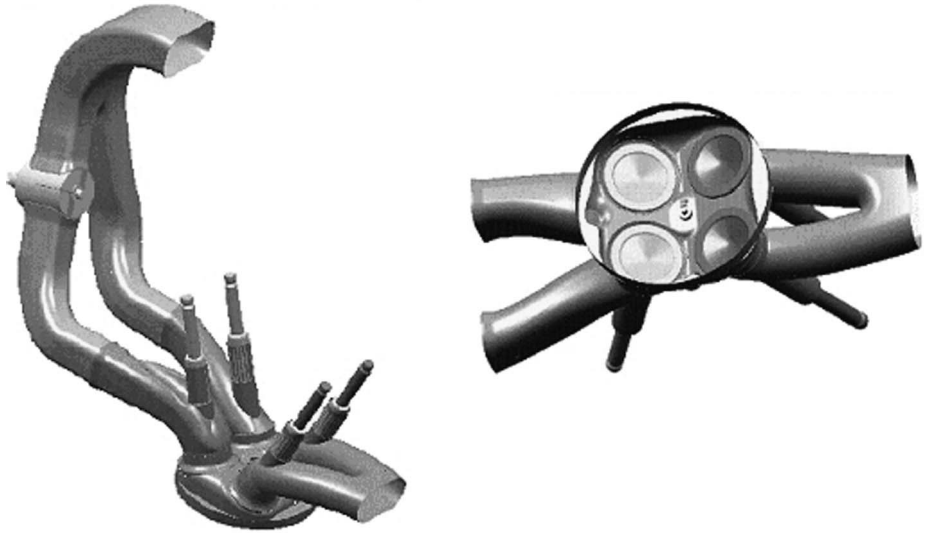

Fig. 9. CAD of combustion Chamber Lay Out.

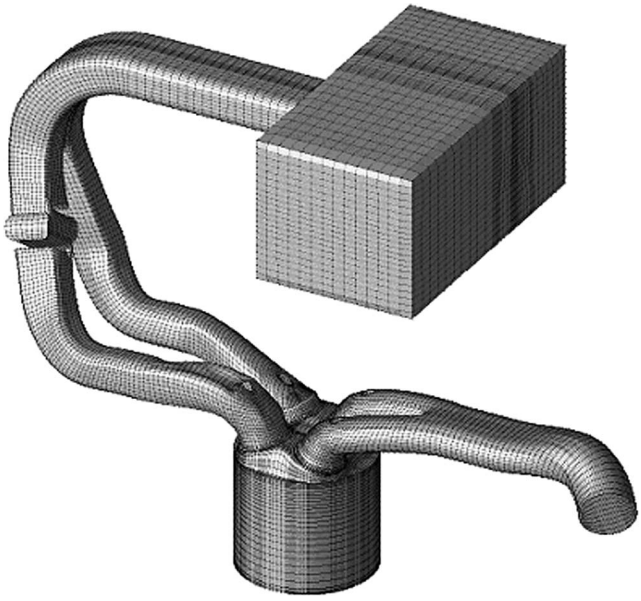

Fig. 10. Computational grid.

analyzed using appropriate nets of the data explorer visualization code [37].

To reach numerical convergence five engine revolutions were necessary for each operating point. The simulation was assumed to converge when the difference between the volumetric efficiencies of two following engine cycles was less then 5%. As boundary conditions at the inlet and outlet of the system a constant in space and time-varying pressure was imposed referring to experimental data. In the following some results for the homogeneous and stratified case are illustrated. In Table 4 the different case operating conditions are reported.

The numerical engine cycle and the four experimental ones related to the different cylinders are reported in Fig. 11. It appears evident that there is a non-uniformity between the

Table 4
Engine operating conditions

Case	RPM	I.M.E.P. [Mpa]	EGR [%]	Swirl	λ	Spark advance
1	3000	0.6	10	OFF	0.954	21.4°
2	3000	0.4	10	OFF	0.953	21.4°
3	4000	0.1	10	OFF	0.983	26.4
4	4000	0.2	10	OFF	0.978	28.5
5	3000	0.1	20	ON	2.04	28.3
6	3000	0.2	10	ON	2.07	27.3

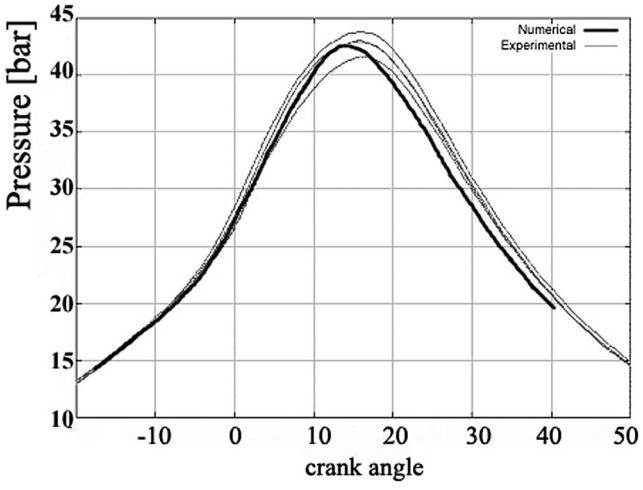

Fig. 11. Experimental and numerical pressure versus crank angle (case 1).

four experimental cycles even though they are averaged between 256. This is due to the different air-spray interaction in the different cylinders that determines different air–fuel mixing also in the homogeneous case. In this engine a triangular shaped plenum (not symmetric respect to the different cylinders) enhances this phenomenon. In any case analyzing the figure it can be evinced that the code very well predicts the ignition delay and the first part of the combustion, whereas it predicts a lower pressure history in the during the expansion

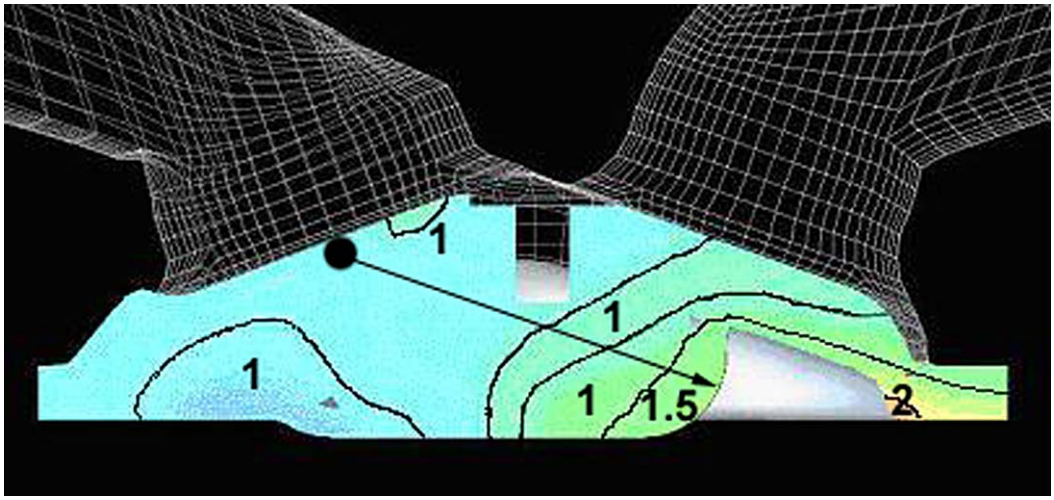

Fig. 12. λ distribution in a plane.

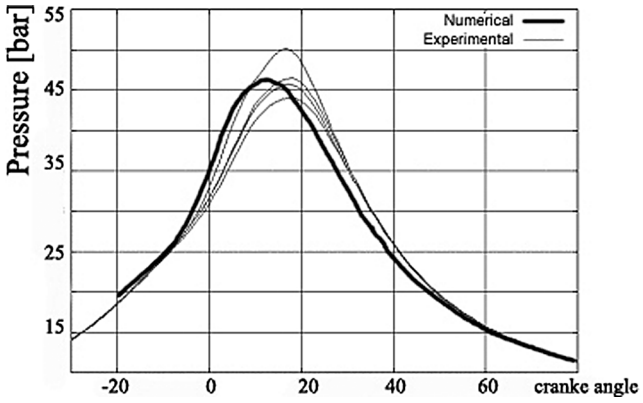

Fig. 13. Pressure history case 2.

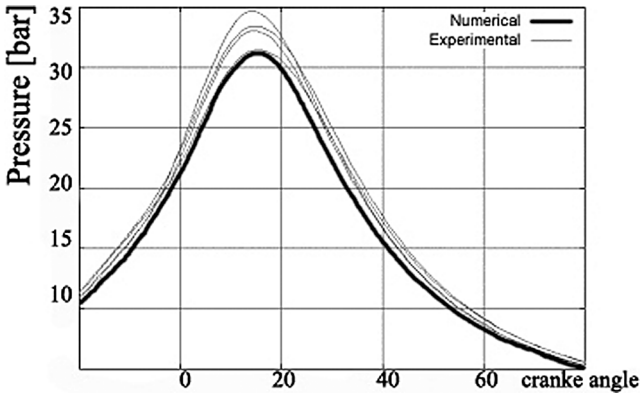

Fig. 14. Pressure history case 3.

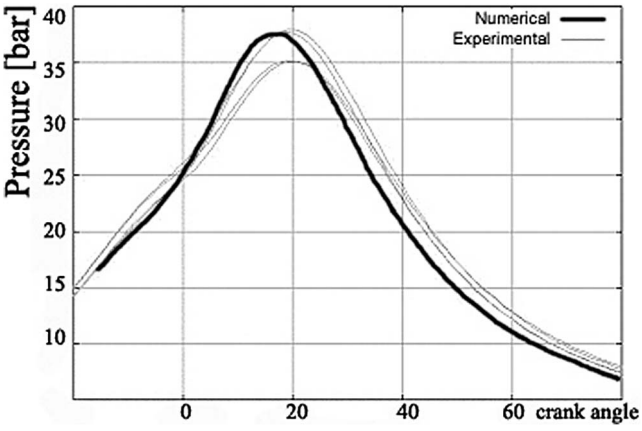

Fig. 15. Pressure history case 4.

stroke. This is due to a wrong estimation of heat transfer and light-off.

The equivalence ratio λ is defined as the ratio between the air/fuel ratio of a mixture and its value at stoichiometric conditions. In Fig. 12 the numerical distribution of λ in a plane containing the cylinder axis is shown for case 1. It is a homogeneous case so there is no charge stratification and the air–fuel ratio is nearly stoichiometric ($\lambda = 1$). On the left side of the chamber, opposite to the injector location (black circle), a strong variation of λ can be seen. In that zone the mixing is not good and there is a strong λ variation. So in this engines, as underlined before, the homogeneous charge case does not mean 'perfect mixing' but only stoichiometric amount of fuel injected. In Fig. 12 it can be also noted that the spark plug has been discretized. The discretization of the volume occupied by the plug highly influences the air motion in the neighbor computational cells. The air velocity in these cells determines the energy transfer efficiency from the plasma to the mixture and velocities higher than 15 $m \cdot s^{-1}$ can determine mis-ignition [38].

In Figs. 13–16 the indicated cycle for case 2–5 are reported. The combustion delay is well modeled in all cases, whereas some discrepancies can be noted for the pressure maximum and expansion stroke pressure history.

Referring to case 5, in Figs. 17 and 18 λ mean values in different spheres centered in the plug are reported, for simulations modeling the spark plug (case a) and not (case b) respectively. Spark timing is 29 degrees BTD, so the engine crank angle at which the stratification level has to be

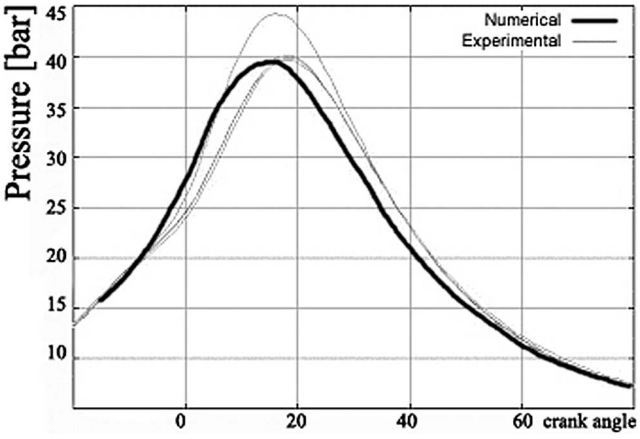

Fig. 16. Pressure history case 5.

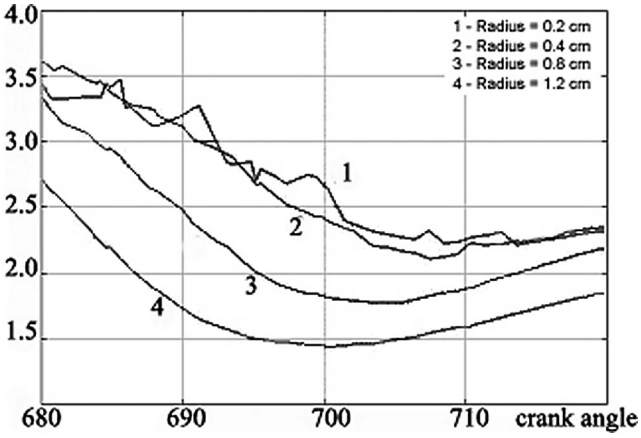

Fig. 17. λ near spark plug (case a).

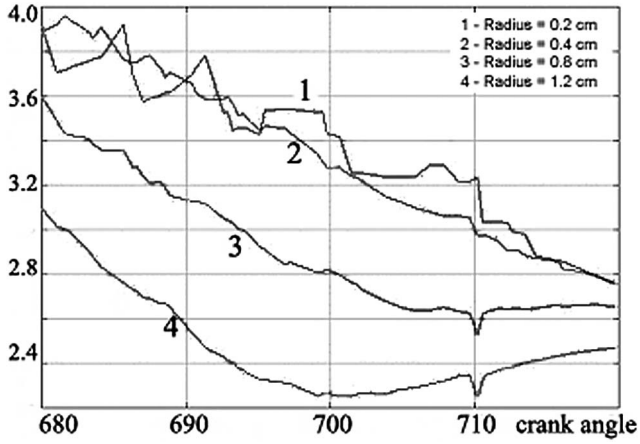

Fig. 18. λ near spark plug (case b).

monitored is 691. A stoichiometric mixture around the spark plug has to be formed in order to obtain ignitable conditions. Moving away from the spark plug the mixture becomes leaner with subsequent reduction in the laminar flame front speed which is balanced by the pressure and temperature variation effects, due to the combustion of the initial stoichiometric mixture.

Comparing Figs. 17 and 18 it is evident that the discretization of the spark volume determines a variation of λ near the plug at the spark ignition timing that varies from 2.45 (case b), not ignitable value, to 1.6 (case a) which is in the flammability range.

7. Conclusions

In present work a model for a GDI high-pressure hollow-cone injector atomization model was validated. At the injector exit the liquid sheet is discretized with numerical *blobs* having characteristic diameter equal to the sheet thickness. This primary blobs breakup following the primary atomization model by Nagaoka and Kawamura [19,25]. The model, after certain conditions are reached, breaks up the primary blobs in smaller secondary droplets whose diameter is determined by the Rosin–Rammler distribution function with a characteristic size related to the size of the ligaments that form on the surface of the annular sheet. For the droplet secondary breakup a hybrid model was used in which different approaches are followed as the droplet Weber number changes. This can be regarded as an innovative approach not used before for gasoline applications, since previous approaches [17,19] only considered primary breakup, probably due to the lower injection pressures of the first generation GDI injection systems. To validate the code two different test were performed in a quiescent chamber at ambient conditions and in a real GDI engine.

(1) The first test has evidenced the predictive capability of the model to evaluate the spray tip penetration in quiescent chamber and the spray temporal shape evolution. Moreover phenomena related to the secondary breakup break-up are well captured by the code.
(2) The second test, concerning the whole engine has shown the possibility to use the numerical tool for both homogeneous and stratified mode. For the stratified charge operating mode, it has been shown how a correct discretization of the chamber (plug volume and valves) is necessary in order to obtain a correct degree of charge stratification inside it. It must be underlined that it is not possible to obtain such information experimentally, so, in this case, the numerical investigation is the only tool available for research.

References

[1] F.F. Zhao, D.L. Harrington, M.C. Lai, Automotive Gasoline Direct-Injection Engines, SAE, 2002.
[2] F.Q. Zhao, M.C. Lai, D.L. Harrington, A review of mixture preparation and combustion strategies for spark-ignited direct injection casoline engine, SAE 970627.
[3] Y. Iwamoto, K. Noma, O. Nakayama, T. Yamauchi, H. Ando, Development of gasoline direct injection engine, SAE 960627.

[4] M. Kanda, T. Baika, S. Kato, M. Iwamuro, Application of a new combustion concept to direct injection gasoline engine, SAE 2000-01-0531.
[5] Y. Tagagi, The role of mixture formation in improving fuel economy and reducing emissions of automotive S.I. engines, FISITA Technical Paper No. P0109, 1996.
[6] M. Kussel et al., Motronic MED7 for gasoline direct injection engines: control strategies and calibration procedures, SAE 1999-01-1284, 1999.
[7] A. Amsden, KIVA-3: A KIVA Program with Block-Structured Mesh for Complex Geometries, Los Alamos National Laboratory, 1993.
[8] A.A. Amsden, J.D. Ramshaw, P.J. O'Rourke, J.K. Dukowicz, A computer program for two and three dimensional fluid flows whit chemical reaction and fuel spray, Los Alamos Labs., LS 12503 MS, 1993.
[9] L. Allocca, F.E. Corcione, S. Golini, F. Papetti, Measurement and modeling of spray/wall dynamics and heat transfer, in: 3rd Int. Kiva Users Meeting, SAE Congress, Detroit, MI, 1993.
[10] H. Ando, Mitsubishi GDI engine—Strategies to meet the European requirement, in: Proceedings from Engine and Environment, Graz, September 1997.
[11] Y.H. Kang, I.-P. Chang, K.M. Jay, A comparison of boundary layer treatments for heat transfer in IC engines, SAE Paper 900252, 1990.
[12] M. Pontoppidan, G. Gaviani, G. Bella, V. Rocco, Direct fuel injection—A study of injector requirements for different mixture preparation concepts, SAE Paper 970628.
[13] M. Pontoppidan, G. Gaviani, G. Bella, V. Rocco, Experimental and numerical study of fuel spray behavior to optimize charge motion in direct injected SI-engine, in: 3rd International ICE Conference on Internal Combustion Engines, Capri, September 1997.
[14] R.D. Reitz, Assessment of wall heat transfer models for premixed-charge engine combustion computations, SAE Paper 910267.
[15] R.D. Reitz, T.W. Kuo, Modelling of HC emissions due to crevice flows in premixed charge engines, SAE Paper 892085.
[16] N.K. Rizt, A.H. Lefebvre, Internal flow characteristics of simplex swirl atomizers, AIAA J. Propulsion Power 1 (1985) 182.
[17] Z. Han, S. Parrish, P.V. Farrel, R.D. Reitz, Modeling atomization processes of pressure swirl hollow-cone fuel sprays, Atomization and Sprays 7 (1997) 663–684.
[18] L. Allocca, G. Bella, A. De Vita, L. Di Angelo, Experimental validation of a GDI spray model, SAE Paper 2002-01-1137.
[19] M. Nagaoka, K. Kawamura, A deforming droplet model for fuel spray in direct-injection gasoline engines, SAE 2001-01-1225, 2001.
[20] N. Dombrowski, D. Hasson, D. Ward, Chem. Engrg. Sci. 12 (1960) 35–50.
[21] N. Dombrowski, D. Johns, The aerodynamic instability and disintegration of viscous liquid sheets, Chem. Engrg. Sci. 18 (1963) 203–214.
[22] J. Sauter, Determining size of drops in fuel mixture of internal combustion engines, NACA TM 390, 1926.
[23] W. Ohnesorge, Formation of drops by nozzles and the breakup of liquid jets, Z. Angew. Math. Mech. 16 (1936) 355–358.
[24] M. Hayakawa, S. Takada, K. Yonesige, M. Nagaoka, K. Takeda, Fuel spray simulation of a slit nozzle injector for direct-injection gasoline engine, SAE 2002-01-1135, 2002.
[25] M. Beccaria, G. Bella, R. Lanzafame, Simulazione fluidodinamica di uno spray di combustibile per motori ad accensione comandata GDI, ATI 2003.
[26] R. Rotondi, G. Bella, C. Grimaldi, L. Postrioti, Atomization of high-pressure diesel spray: Experimental validation of a new breakup model, SAE Paper 2001-01-1070, 2001.
[27] E. Giffen, A. Muraszew, The Atomisation of Liquid Fuels, Chapman & Hall.
[28] G. Brower, S.K. Chang, M.L. Corradini, M. El-Beshbeeshy, J.K. Martin, J. Krueger, Physical mechanism for atomization of a jet spray: A comparison of models and experiments, 881318 SAE Paper, 1988.
[29] G.L. Borman, Combustion Engineering, McGraw-Hill, New York, 1998.
[30] R.D. Reitz, Computer modeling of sprays, in: Spray Technology Short Course, Pittsburgh, PA, May 1996.
[31] P.J. O'Rourke, A.A. Amsden, The tab method for numerical calculation of spray droplet breakup, 872089 SAE Paper, 1987.
[32] E.A. Ibrahim, H.Q. Yang, A.J. Przekwas, Modeling of spray droplets deformation and breakup, AIAA J. Propulsion Power 9 (1993) 651–654.
[33] G. Bella, R. Rotondi, F.E. Corcione, G. Valentino, Experimental and computational analysis of a diesel spray, in: 4th International Conference ICE99, Internal Combustion Engines: Experiments and Modeling, Capri, 1999.
[34] A. Devita, M. Alaggio, R. Rotondi, Experimental and numerical studies of diesel fuel and biodiesel spray, ASME Technical Paper, 2000.
[35] M.I.D.I. Nu, A private comunications, 2003.
[36] S. Paoletti, ENGAGE a multi-block environment for grid generation, in: ICIAM 95, Third International Congress on Industrial and Applied Mathematics, Hamburg, Germany, July 3–7, 1995.
[37] http://www.opendx.com.
[38] R. Herweg, R. Maly, A fundamental model for flame kernel formation in S.I. engines, SAE Paper 922243.